*Geobiology*

WILEY

gebiology

ORIGINAL ARTICLE

# How to Make a Rock in 150 Days: Observations of Biofilms Promoting Rapid Beachrock Formation

Brianna M. Hibner[1] | Marjorie D. Cantine[2] | Elizabeth J. Trower[1] | Jacqueline E. Dodd[3] | Maya L. Gomes[3]

[1]Department of Geological Sciences, University of Colorado Boulder, Boulder, Colorado, USA | [2]Department of Earth and Space Sciences, University of Washington, Seattle, Washington, USA | [3]Department of Earth and Planetary Sciences, Johns Hopkins University, Baltimore, Maryland, USA

**Correspondence:** Brianna M. Hibner (brianna.hibner@colorado.edu) | Marjorie D. Cantine (cantine@uw.edu) | Elizabeth J. Trower (lizzy.trower@colorado.edu)

**Received:** 12 July 2024 | **Revised:** 15 October 2024 | **Accepted:** 13 January 2025

**Funding:** This work was supported by National Science Foundation, OCE-2032129 and OCE-2307830.

## ABSTRACT

Beachrock is a type of carbonate-cemented rock that forms via rapid cementation in the intertidal zone. Beachrock is a valuable geological tool as an indicator of paleoshorelines and may protect shorelines from erosion. Previous studies present a range of hypotheses about the processes enabling rapid beachrock formation, which span purely physicochemical mechanisms to a significant role for microbially mediated carbonate precipitation. We designed a set of in situ field experiments to explore the rates and mechanisms of beachrock formation on Little Ambergris Cay (Turks and Caicos Islands). Our field site has evidence for rapid beachrock cementation, including the incorporation of 20th century anthropogenic detritus into beachrock. We deployed pouches of sterilized ooid sand in the upper intertidal zone and assessed the extent of cementation and biofilm development after durations of 4 days, 2.5 months, and 5 months. We observed incipient meniscus cements after only 4 days of incubation in the field, suggesting that physicochemical processes are important in driving initial cementation. After 2.5 months, we observed substantial biofilm colonization on our experimental substrates, with interwoven networks of *Halomicronema* filaments binding clusters of ooids to the nylon pouches. After 5 months, we observed incipient beachrock formation in the form of coherent aggregates of ooids up to 1 cm in diameter, bound together by both networks of microbial filaments and incipient cements. We interpret that the cyanobacteria-dominated beachrock biofilm community on Little Ambergris Cay plays an important role in beachrock formation through the physical stabilization of sediment as cementation proceeds. Together, this combination of physicochemical and microbial mechanisms enables fresh rock to form in as little as 150 days.

## 1 | Introduction

Carbonate sedimentary rocks begin as sediments precipitated, with or without biological mediation, from Earth surface fluids, including seawater, meteoric waters, and groundwater. Further precipitation of cements within pore spaces can lithify carbonate sediments in surface environments, prior to any burial or compaction. Specific petrographic phases within carbonate rocks reflect this type of (nearly) syn-sedimentary cementation, such as gravitational fabrics (e.g., dripstone, pendant, and meniscus cements) or hardground cements (Flügel 2010). Anthropogenic inclusions in carbonate rocks, such as ancient Greek pottery in submarine hardgrounds (Shinn 1969) and Coca-Cola bottles in beachrock (Davies and Kinsey 1973), suggest that the pace of syndsedimentary lithification can be rapid across multiple depositional environments.

This study explores the processes responsible for the rapid lithification of beachrock—or carbonate-cemented rock composed of beach sediment that forms at shorelines—in a study site in

Brianna M. Hibner, Marjorie D. Cantine and Elizabeth J. Trower contributed equally to this study.

the Turks and Caicos Islands. Beachrock can form quickly (McCutcheon et al. 2017; Falkenroth et al. 2022), and elucidating the rate of beachrock formation and the processes responsible is valuable for a number of applications in the Earth sciences. Beachrock is widely used as an indicator of paleoshoreline location in studies of sea level and uplift (Mauz et al. 2015). Furthermore, beachrock may help to armor and protect vulnerable coastlines (Cooper 1991; Dickinson 1999), so the ability to trigger, control, or promote its rapid formation could be a valuable tool for coastal management.

The relative contributions of physiochemical and biological mechanisms responsible for beachrock formation are not fully understood. The processes responsible may vary between locations (Vousdoukas, Velegrakis, and Plomaritis 2007). The latitudinal distribution of beachrock—concentrated at latitudes below 40°—suggests that the same physiochemical controls that govern carbonate precipitation more broadly (e.g., temperature, alkalinity) are important (Vousdoukas, Velegrakis, and Plomaritis 2007). Physiochemical processes invoked in beachrock formation include carbonate precipitation directly from meteoric or marine waters (Ginsburg 1953; Gischler and Lomando 1997) or mingled meteoric-marine fluids (Moore Jr 1973; Hanor 1978), potentially enhanced by $CO_2$ degassing (Hanor 1978). Some observations support the importance of microbial involvement in beachrock formation, especially in regard to the role of microbial biofilms as loci for cementation (Neumeier 1999; McCutcheon et al. 2016, 2017). Petrographic characterization of beachrock from Heron Island, Australia, identified the paired processes of microbial dissolution of carbonate during boring and the precipitation of aragonite cements within microbial extracellular polymeric substances (EPS) as key to the lithification of beachrock in that system (McCutcheon et al. 2016). Under laboratory conditions meant to mimic natural conditions, carbonate sediments inoculated with microbes formed incipient beachrock with close association of microbial biofilm and cements (McCutcheon et al. 2017), suggesting that, at least in some settings, physiochemical processes of evaporation and tidal cycling may be less important than the microbial contributions to early cementation and lithification. This study sets out to describe both microbial and physiochemical contributions to beachrock formation using an in situ approach in a field area where observations indicate that beachrock forms rapidly.

### 1.1 | Study Site: Little Ambergris Cay

Little Ambergris Cay is a protected nature reserve, administered by the Department of Environmental and Coastal Resources of the Turks and Caicos Islands and the Turks and Caicos National Trust. It is a small (6.1 $km^2$) island on the Caicos Platform (Figure 1a–c). Rock exposures on Little Ambergris Cay are Holocene in age, with no evidence for Pleistocene outcrop or antecedents (Orzechowski, Strauss, and Knoll 2016; Cantine et al. 2024). The interior of the island is covered by a mangrove-microbial mat-dominated tidal swamp. The perimeter of the island consists of a rim of lithified dunes, beachrock, and unlithified shoreline (Figure 1c) (Stein et al. 2023; Cantine et al. 2024). Ooids make up the bulk of sediment, both lithified and unlithified, on Little Ambergris Cay with some minor contributions from skeletal carbonates.

Beachrock is common along the southern coast of the island, including a strandplain of beach ridges (Figure 1c) and well-exposed coastal outcrops (Cantine et al. 2024). Aeolianite dunes are also lithified and well-exposed, especially on the northern shore of the island. Although these dunes are lithified, we do not identify them as *beachrock*, which we reserve exclusively for lithified sediments formed at the shoreline.

Some beachrock on Little Ambergris Cay is horizontal- to seaward-dipping planar-laminated fossiliferous oolite deposited in the upper foreshore environment (Figure 1d,e). Beachrock consisting of monomict carbonate breccias with meter-scale clasts of aeolian and foreshore ooid grainstones in ooid grainstone matrix are also common in the intertidal zone (Figure 1f,g). The clasts within are occasionally imbricated. Each individual breccia unit is locally developed and is up to 5 m in width. The coherence and shape of breccia clasts show that they were lithified prior to incorporation into breccias; these breccia units therefore document multiple generations of lithification and cementation. Radiocarbon data on shells and sediment from both lithified foreshore and breccia deposits indicate that lithification is recent (within the last 1000 years) and ongoing (Cantine et al. 2024). Beachrock on Little Ambergris Cay sometimes includes anthropogenic debris, including 20th-century glass bottles and jars (Figure 1g) (Cantine et al. 2024).

Some differences between beachrock and aeolianites on Little Ambergris Cay highlight a potential role for microbial contributions to beachrock lithification. By definition, beachrock forms within the intertidal zone. On Little Ambergris Cay, a surficial black biofilm is closely associated with rocks in the intertidal zone, and this biofilm is not observed on lighter-colored overlying rock (Figure 2a). Beachrock on Little Ambergris Cay is also better cemented at exposed surfaces than overlying aeolianite. Where fresh surfaces of beachrock are exposed, an internal rind of green biofilm along surfaces exposed to light can be observed (Figure 2b); no such green biofilm is found within aeolianites. These observations are consistent with the presence of a photosynthetic and endolithic microbial consortium within beachrock and the absence of this community within other lithified sediments above the intertidal zone. In these respects, Little Ambergris Cay beachrock is similar to Heron Island beachrock; previous studies have interpreted that the biofilm and endolithic microbial community contribute to the formation of beachrock on Heron Island (McCutcheon et al. 2016, 2017). Here, we describe the microbial community present within Little Ambergris Cay beachrock and explore its contribution to beachrock formation. This study also constrains the rate of beachrock formation under field conditions on Little Ambergris Cay through a suite of in situ field incubation experiments.

## 2 | Materials and Methods

### 2.1 | Experimental Design

We designed an in situ field experiment to track biofilm colonization and incipient carbonate mineral cementation by deploying replicates of sterilized ooid sand for incubation over periods of increasing duration. We sieved ooid sand that had been previously collected from Ambergris shoal

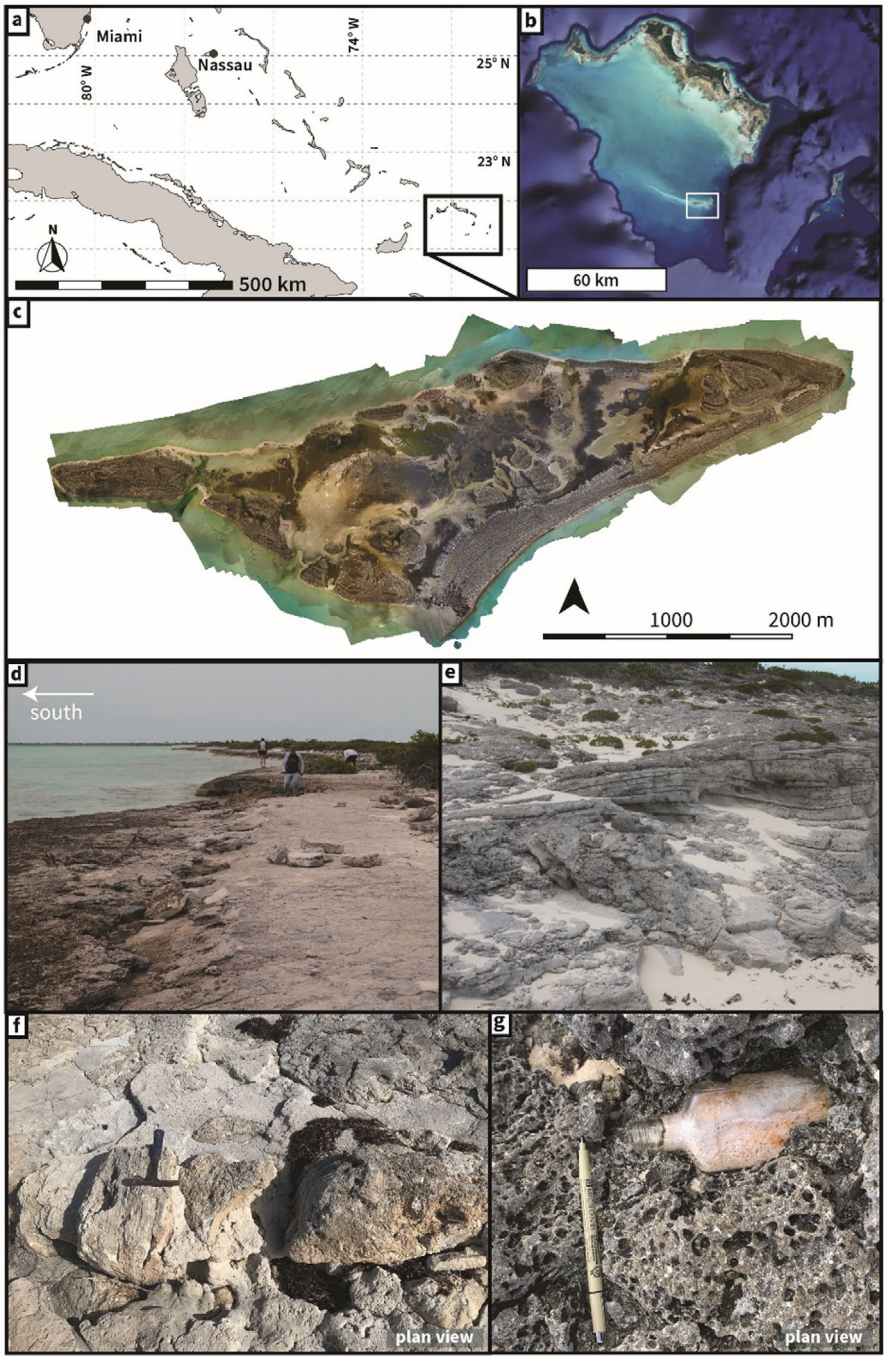


**FIGURE 1** | Location and key facies of Little Ambergris Cay, Turks and Caicos Islands. (a) Location of the Turks and Caicos Islands, marked with a black rectangle, within the region. (b) Satellite imagery of the Caicos Platform. Imagery from Google Earth. Location of Little Ambergris Cay marked with white rectangle. (c) Orthomosaic imagery of Little Ambergris Cay from July 2016 (Stein et al. 2023). The compass arrow points north. (d) Prograding beachrock deposits on the southern coast of Little Ambergris Cay. Photo credit: E. Orzechowski. (e) Horizontal to seaward-dipping beachrock overlain by aeolianite. View is landward. Photo credit: A. Knoll. (f) Reworked boulders and cobbles in conglomerate. Rock hammer for scale. Photo credit: M. Cantine. (g) Some conglomeratic beachrock on Little Ambergris Cay contains anthropogenic debris, including glass bottles like this one. Photo credit: M. Cantine.

(a ~20-km-long ooid shoal extending to the west of Little Ambergris Cay) to a 250–500 μm fraction. We sterilized the sand by autoclaving it at 121°C for 2 h. The primary goal of sterilization was to eliminate native microbes that might flourish when they were returned to their preferred environment on Little Ambergris Cay. We divided sterilized sediment into 24 15-mL replicates and then analyzed grain size and shape distributions of each sample via Retsch Camsizer P4. We then funneled 23 of these replicates into individual pouches created from 75-μm mesh nylon (commercially sold as culinary cloth sieves), heavy-duty nylon thread, and Gear Aid Seam Grip WP seam sealer (Figure 3). This mesh size was selected to maximize connectivity for water and microbes to filter through the nylon while also keeping the sand within

the pouch. The sand was not tightly packed in each pouch, such that grains could easily shift around one another when the pouch was shaken (such as when it might be rolled around by waves at high tide). Replicate 24 was retained in the lab in a 15-mL centrifuge tube as a control. Each pouch of sand was inserted into a 4.5-cm-diameter rubber polyhedral meshwork ball (commercially available as a dog toy) to protect it from abrasion by the existing beachrock. Pouches were redundantly labeled with thread, the color of the enclosing dog toy, and color-coded zip ties.

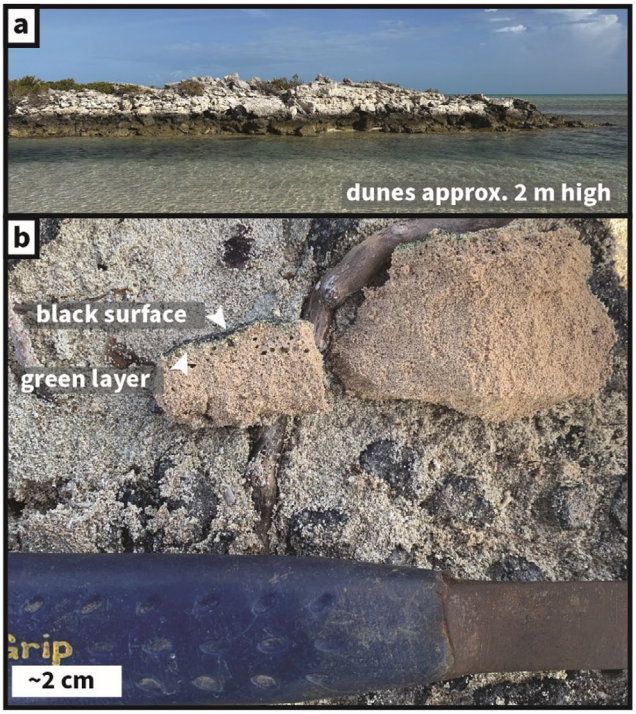


**FIGURE 2** | Features of beachrock on Little Ambergris Cay. (a) View of shoreline on Little Ambergris Cay, including beachrock, boulder rubble, and overlying aeolianite. Rocks exposed at the shoreline, including beachrock, have a black surface color; compare to lithified sediments above the intertidal zone, which are compositionally identical but lack the black surface color. Photo credit: M. Cantine. (b) A thin green biofilm is found at the upper surface, just under the blackened surface, of freshly exposed beachrock. Photo credit: M. Cantine.

We traveled to Little Ambergris Cay in February 2023 to deploy our experiment in the field. We selected a site for deploying the experiment that met the following criteria:

1. Located in the upper intertidal zone, such that samples were only submerged briefly at high tide. The tides on Little Ambergris Cay are semidiurnal: there are two high tides per day of unequal magnitude, the asymmetry of which changes throughout the lunar cycle. Our site was located such that it was submerged by the higher high tide, but not necessarily submerged by the lower high tide.
2. Located on or adjacent to existing biofilm-covered beachrock.
3. Located adjacent to recent anthropogenic detritus cemented into beachrock.

At our selected field site, we used glue-in stainless-steel rock-climbing bolts to secure three lanyards of sample pouches to the existing beachrock. Each lanyard comprised seven or eight pouches, which were attached together with both marine-grade nylon paracord and plastic-coated stainless-steel lanyards (Figure 3).

We collected samples after deployment at three time points: 4 days, 2.5 months, and 5 months of incubation time in the field. No hurricanes passed over the study site during our observational period. At each sampling time point, we collected four replicates of each sample: one replicate was subsampled for 16S rRNA analysis and microscopy and three replicates were prepared for grain size and shape analysis. At the 2.5 month and 5 month time points, we collected two additional replicates for total organic carbon (TOC) analyses.

## 2.2 | Grain Size Analyses

At each time point, three replicates were prepared for grain size analysis by rinsing and drying sediment the same day they

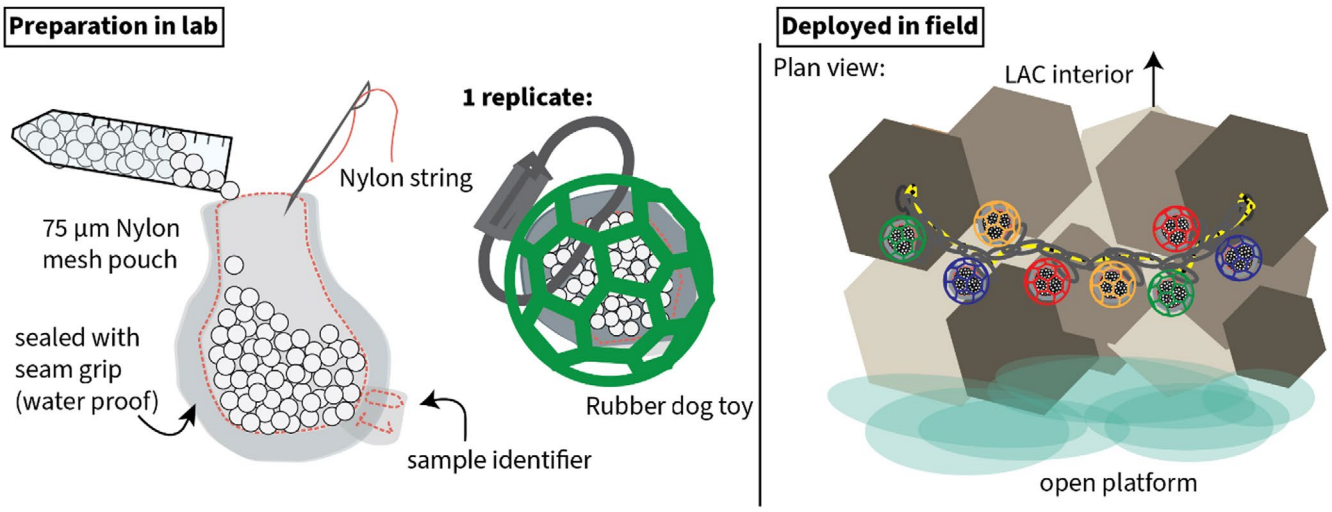


**FIGURE 3** | Schematic of experimental design.

were collected from the field. Dry samples were analyzed for distributions of grain size and shape via Retsch Camsizer P4. Distributions of size and shape parameters of each individual sample were compared with analyses of that sample prior to deployment in the field.

### 2.3 | DNA Extraction

At each time point, two subsamples from one replicate were prepared for 16S rRNA gene sequencing by using a sterilized spatula to scoop sediment from inside the pouch into a 1.5 mL Qiagen Powersoil Pro bead tube pre-filled with 600 μL of RNAlater. Cells were lysed by bead-beating, and microtubes were stored frozen. The DNA samples were defrosted, vortexed for approximately 5 s, centrifuged for 1 min at 15,000 RCF at room temperature, and the RNAlater supernatant was removed via pipette. Samples were then washed with 800 μL of Dulbecco's phosphate-buffered saline (dPBS), vortexed for approximately 5 s, centrifuged for 1 min at 15,000 RCF at room temperature, and the dPBS supernatant removed via pipette. DNA was then extracted using the Qiagen DNeasy PowerSoil Pro Kit following the manufacturer's protocol.

### 2.4 | Library Preparation

The V4 region of the 16S rRNA gene was amplified via polymerase chain reaction (PCR) with a two-step protocol. Real-time PCR was performed as 25 μL reactions in duplicate to group samples by approximate DNA template concentrations, thus avoiding thermocycling past the mid-linear phase. This resulted in two groups of samples. One group cycled for 18 cycles, and the other cycled for 25 cycles. Master mix for qPCR and step 1 PCR was prepared by hand using the following reagents per 25 μL reaction: Nuclease Free Water 12.125 μL, HF Buffer 5 μL, 10 μM dNTPs 0.5 μL, 3 μM forward and reverse primers 2.5 μL, Phusion 0.25 μL, DNA template 2 μL. For real-time PCR, 0.125 μL of a 1/100 dilution of SYBR Green was added, and 0.125 μL of Nuclease Free Water was removed to maintain 25 μL volume per reaction. For qPCR and step 1 PCR, samples used the following primers: PE16S_V4_U515_F: 5′ ACACG ACGCT CTTCC GATCT YRYRG TGCCA GCMGC CGCGG TAA-3′, and PE16S_V4_E786_R: 5′ CGGCA TTCCT GCTGA ACCGC TCTTC CGATC TGGAC TACHV GGGTW TCTAA T 3′ (Preheim et al. 2013). Samples were cycled using the following conditions: denaturation at 98°C for 30 s, annealing at 52°C for 30 s, and extension at 72°C for 30 s. For step 2, PCR Master mix was prepared by hand using the following reagents per 25 μL reaction: Nuclease Free Water 8.65 μL, HF Buffer 5 μL, 10 μM dNTPs 0.5 μL, 3 μM forward and reverse Primers 3.3 μL, Phusion 0.25 μL, DNA template 4 μL. Step 2 PCR samples used an eight base pair barcode complete with Illumina adapter sequences, and samples were cycled for nine cycles using the following thermocycler conditions: denaturation at 98°C for 30 s, annealing at 83°C for 30 s, and extension at 72°C for 30 s. Step one and step two PCR 25 μL reactions were run in quadruplicate, then pooled and cleaned with Beckman Coulter Agencourt AMPure XP Bead-Based Reagent using 95 μL of DNA template and 85 μL of AMPure XP Bead-Based Reagent, otherwise following the manufacturer's directions. DNA assays were performed using the Invitrogen Qubit 1× dsDNA High Sensitivity Kit prior to sequencing to confirm PCR amplification success.

### 2.5 | Sequencing

The libraries were multiplexed with unrelated libraries not used in this study and underwent paired-end sequencing on the Illumina MiSeq platform at The Johns Hopkins University of Medicine Genetic Resources Core Facility (GRCF).

### 2.6 | Sequencing Data Analysis

All sequence data was demultiplexed using QIIME2 version 2023.5 and denoised with DADA2 prior to filtering samples exclusively from this project for downstream analysis (Callahan et al. 2016; Bolyen et al. 2019). Primers were trimmed, and sequences were truncated at 200 base pairs based on quality scores. Taxonomic assignment of amplicon sequence variants was performed using the q2-feature classifier (Bokulich et al. 2018), a QIIME 2 plugin, and a pre-trained Naive Bayes taxonomic classifier using Greengenes version 13_8 (McDonald et al. 2012). Sequence alignment was performed using Mafft (Katoh et al. 2002), and FastTree (Price, Dehal, and Arkin 2010) was used to generate a phylogenetic tree.

### 2.7 | Light and Electron Microscopy

Four subsamples of one replicate from each time point and two samples of in situ beachrock adjacent to the experiment site were prepared for microscopy. Immediately after collection, samples were fixed with paraformaldehyde and dehydrated in a series of decreasing dilutions of ethanol with 1× phosphate-buffered saline (PBS). Fixed and dehydrated samples were stored in 100% EtOH for transport back from the field site. At the University of Colorado Boulder, aliquots of each microscopy sample were placed in flat-bottom size 00 polyethylene capsules and embedded in LR White resin through a series of infiltration steps of increasing concentration: 50% LR White in EtOH, 75% LR White in EtOH, 90% LR White in EtOH, 95% LR White in EtOH, and three infiltrations of 100% LR White in EtOH. Each infiltration step was incubated for ~24 h. In the final step, accelerator was added to the resin prior to pipetting into capsules; filled capsules were sealed with parafilm and placed in a 0°C fridge to polymerize overnight. Embedded samples were removed from capsules and trimmed to size with a gem saw or polished down with sandpaper, then submitted to Grindstone Laboratory (Portland, OR) for preparation as polished thin sections.

Thin sections were examined using plane- and cross-polarized transmitted light with a Zeiss AxioImager M2 equipped with a 6MP 33fps Axiocam 506 color camera. Raman spectra were collected using a Horiba LabRAM HR Evolution Spectrometer with a 785 nm excitation laser at the CU Boulder Raman Microspectroscopy Lab.

Aliquots of each sample that were not embedded and sectioned were mounted on carbon tape for secondary electron microscopy (SEM) using a Hitachi TM-4000PlusE-2 in the Colorado Shared

Instrumentation in Nanofabrication and Characterization (COSINC) at the University of Colorado Boulder. Secondary electron and backscattered electron imaging were conducted at 10 or 15 kV accelerating voltages with working distances of 6–8 mm.

### 2.8 | Organic Carbon Analyses

TOC was analyzed in the CU Boulder Earth Systems Stable Isotope Lab (CUBES-SIL) (RRID:SCR_019300). Two subsamples of ooids were collected from each of two replicates for both the 2.5 month and 5 month time points, resulting in four samples per time point. Four subsamples were extracted from replicate CP7 and 3 subsamples from replicate CP17 for sample error and drift calculations. We also analyzed one control sample that was never deployed and which remained in the home laboratory. Replicates collected at the 4-day time point were rinsed prior to TOC analyses and were analyzed with another dataset of rinsed subsamples from 2.5 to 5-month time points. Data from these rinsed samples are not included in our results because the comparison of rinsed and unrinsed 5-month samples revealed that the rinsed samples had lower TOC values. Sample preparation steps for organic carbon analyses followed CUBES-SIL protocols and are as follows: A small scoop of ooids was powdered using a mortar and pestle, which was cleaned with 70% isopropyl alcohol and milliQ water between samples. Powders were stored in plastic 1.5 mL microcentrifuge tubes. Combusted flat-bottom 2 mL glass vials were individually labeled and weighed, and then ~2000 μg of powdered ooid sampled was added to each vial. A total of 1910 μL of 6 M HCl was added to acidify each sample in each glass vial over a 1-week duration, starting with a 50 μL addition and increasing with time up to 200 μL. After each acidification step, vials were vortexed for 30 s, un-capped, and placed in a heated bath at 60°C within a fume hood. Once bubbling ceased, each sample was treated with three 500 μL rinses of MilliQ water followed with 24-h heat bath at 60°C in between each rinse. After acidification to remove all $CaCO_3$, samples were air-dried in the fume hood. Once dry, samples were rehydrated with 30 μL of milliQ water and mixed into a slurry using an ultra-sonicator, then centrifuged (2 mL glass tubes were cushioned with Kimwipes to sit snug within a 15 mL centrifuge tube) for 2 min at 1500 rpm. 20 μL aliquots of this slurry were pipetted into pre-weighed tin capsules and dried in an oven for 72 h. Once dry, samples were weighed again, folded into aluminum tins, and analyzed on a Thermo Delta V isotope ratio mass spectrometer (IRMS) coupled to an Elemental Analyzer.

## 3 | Results

### 3.1 | Qualitative Field Observations

Qualitatively, we observed no clear difference after the samples were incubated in the field for 4 days. After 2.5 months of field incubation, we noted that the nylon pouches were noticeably green (Figure 4a,b); however, upon opening the pouches, we observed that the green color was mostly on the nylon, and we did not observe evidence of incipient cementation. After 5 months of field incubation, the nylon pouches were still noticeably green; upon opening the pouches, we observed coherent aggregates of grains ranging from several mm to >1 cm in diameter (Figure 4c), mostly developed in the ~5 mm of sediment adjacent to the nylon pouch. These aggregates stayed coherent even after gentle rinsing.

### 3.2 | Grain Size Analyses

Prior to field incubation, sand samples had median grain diameters ($D_{50}$) ranging from 400 to 424 μm, with 10th percentile grain diameters ($D_{10}$) ranging from 305 to 324 μm and 90th percentile grain diameters ($D_{90}$) ranging from 498 to 516 μm (Table 1). $D_{50}$, $D_{10}$, $D_{90}$, and overall grain size distributions did not change significantly in the 4-day and 2.5-month field incubation samples (Table 1). In the 5-month field incubation samples, $D_{50}$, $D_{10}$, and $D_{90}$ increased for all three samples, and grain size distributions became more positively skewed (Table 1). These results are consistent with our qualitative observations of pieces of incipient beachrock (i.e., larger grains) occurring in every pouch from this time point.

### 3.3 | Microscopy

SEM analyses revealed that the samples that were incubated in the field for only 4 days already had evidence of incipient cementation in the form of isolated scoop-shaped patches of meniscus


**FIGURE 4** | Images of 2.5-month (a, b) and 5-month (c) field incubation samples immediately after retrieval from the field incubation site. (a, b) Images of the pouches after 2.5 months of field incubation show that the inner surfaces of the pouch and the adjacent sediment were noticeably green, but the green biofilm was mostly concentrated along the nylon on parts of the pouch that received the most light. (c) Image of an example of a fragment of incipient beachrock that we retrieved from a pouch after 5 months of field incubation. This sample was fixed in PFA and dehydrated in ethanol for microscopy.

**TABLE 1** | Comparison of grain size distributions before and after field experiments.

| Sample name | Time point | $D_{10}$ (μm) | $D_{50}$ (μm) | $D_{90}$ (μm) | Skewness |
|---|---|---|---|---|---|
| CP_2 | $t=0$ | 325 | 425 | 517 | −0.026 |
| | $t=4$ days | 326 | 424 | 510 | −0.063 |
| CP_3 | $t=0$ | 308 | 404 | 500 | 0.005 |
| | $t=4$ days | 308 | 404 | 500 | 0.000 |
| CP_4 | $t=0$ | 311 | 410 | 504 | −0.016 |
| | $t=4$ days | 310 | 409 | 502 | −0.025 |
| CP_8 | $t=0$ | 308 | 405 | 506 | 0.033 |
| | $t=2.5$ months | 308 | 404 | 498 | −0.002 |
| CP_9 | $t=0$ | 311 | 406 | 502 | 0.014 |
| | $t=2.5$ months | 308 | 403 | 498 | −0.002 |
| CP_10 | $t=0$ | 311 | 406 | 502 | 0.017 |
| | $t=2.5$ months | 305 | 400 | 499 | 0.018 |
| CP_14 | $t=0$ | 311 | 409 | 504 | −0.016 |
| | $t=5$ months | 312 | 411 | 511 | 0.009 |
| CP_15 | $t=0$ | 317 | 413 | 508 | −0.003 |
| | $t=5$ months | 319 | 420 | 533 | 0.236 |
| CP_16 | $t=0$ | 304 | 399 | 499 | 0.024 |
| | $t=5$ months | 315 | 426 | 1165 | 0.523 |

cement (Figure 5a) that were not observed on control samples that were never incubated in the field. We did not observe any pairs of grains that were cemented together by these incipient meniscus cements. These incipient cements were not readily apparent in thin sections of samples, likely because we were able to examine much more surface area in SEM than in thin sections. After 2.5 months, these incipient cement patches were noticeably more abundant (Figure 5b,c). We also observed thin (~1 μm-thick), interwoven microbial filaments after 2.5 months, mostly associated with the nylon mesh, and including coherent aggregates of ooids that were attached to the nylon mesh by these filaments (Figure 5d–f). Again, these fabrics were more readily apparent in SEM than in thin section, both due to the small scale of the features and the greater amount of grain surface area that we could examine via SEM. Locally, these interwoven filaments appeared to substantially reduce the cross-sectional area of the mesh available for seawater to flow through (Figure 5d). However, the majority of the surface of each pouch was not covered by this type of dense biofilm (Figure 4a,b), suggesting that each pouch remained an open system for the duration of the experiment. After 5 months, filaments were much more abundant and more densely interwoven, in many cases forming solid bridges between adjacent grains (Figure 5g–k). As these filament bridges became more densely interwoven, the surface texture became smoother (Figure S1). Mineral precipitation along filaments was also common (Figure 5j). Meniscus cements were large and well-developed enough to be clearly visible in thin section in these samples (Figure 6a–e). In situ beachrock samples were characterized by dense bridges of filaments connecting adjacent grains (Figure 5l, Figure S1), most of which were intensely microbored (Figure 6f,g); these features were clearly visible in both SEM and in thin section.

Raman microspectroscopy revealed that the incipient cements in 5-month field incubation samples were primarily composed of aragonite, with smaller zones composed of high-Mg calcite (Figure S2, Table S1). We were not able to collect Raman spectra on incipient cements from the 4-day or 2.5-month field incubation samples because these cements were too sparse to be captured in thin sections.

### 3.4 | Organic Carbon Analyses

TOC content increased with incubation time. TOC increased from an average of 0.17% ($n=2$) for the control samples to an average of 0.20% ($n=5$) for the 5-month incubation samples. The 2.5-month samples were not significantly different from the control (Figure 7a). $\delta^{13}C_{org}$ values for each time point overlapped, showing no statistically significant change over the duration of this experiment (Figure 7b). Samples that were rinsed with tap water before TOC analysis measured less TOC than unrinsed samples (Table S2).

### 3.5 | Microbial Community Analyses

The microbial communities in the field incubation samples and the in situ beachrock microbial community were primarily composed of Proteobacteria, Actinobacteria, Cyanobacteria,

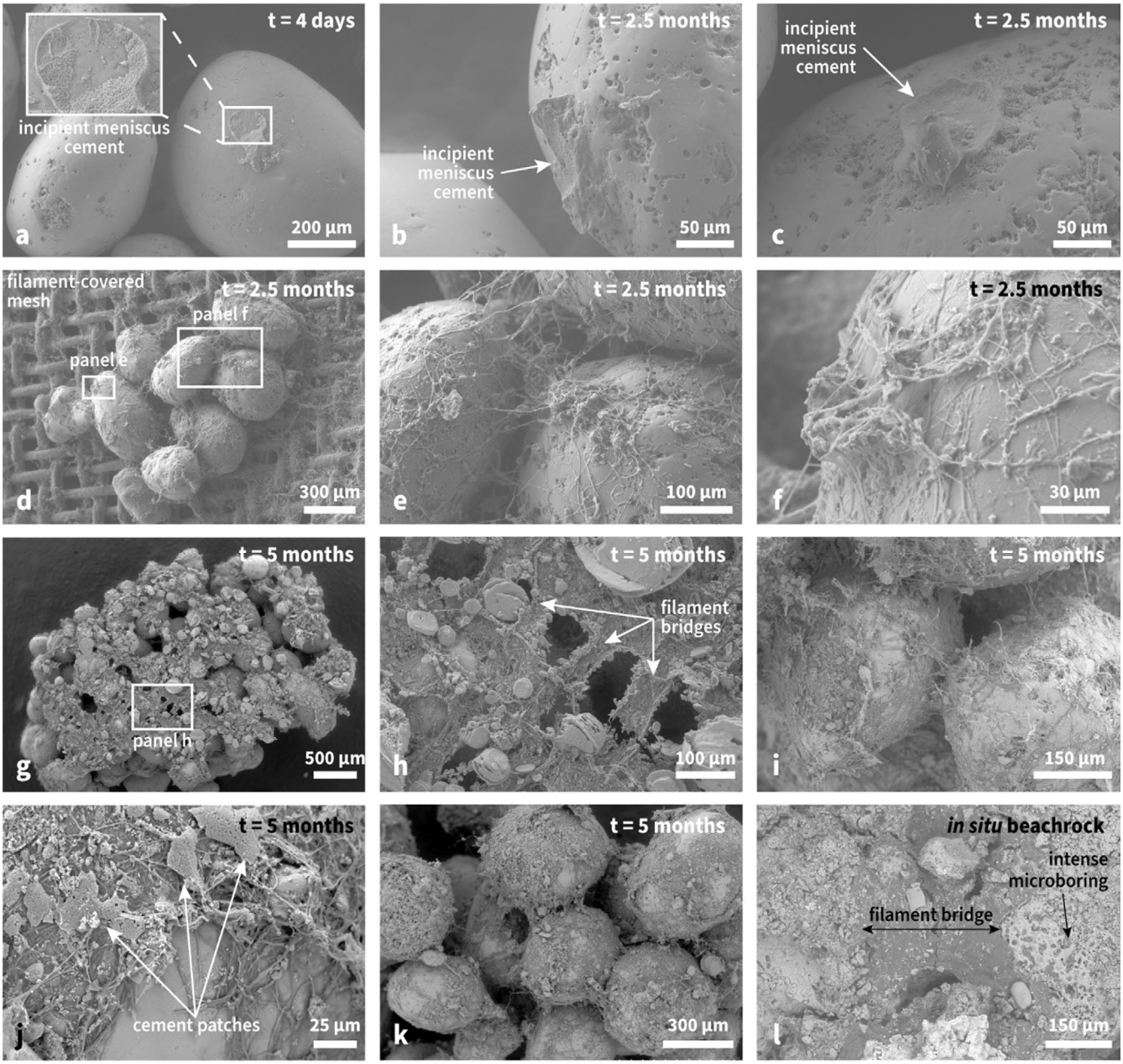


**FIGURE 5** | SEM images of samples from field incubation experiments (a–k) and in situ beachrock. (a) Representative image of samples incubated in the field for 4 days, which were mostly comprised of smooth, polished ooid sand, similar to control sediment. However, we observed some evidence of incipient meniscus cements (inset panel). (b–f) Representative images of samples incubated in the field for 2.5 months. Cup-shaped incipient meniscus cements (b, c) were more common than in samples incubated for 4 days. Interwoven networks of microbial filaments were abundant on the nylon mesh and anchored clusters of ooids to the mesh (d–f). These microbial filaments were not observed on loose ooid sediment from the interior of the mesh bag. (g–k) Representative images of samples incubated in the field for 5 months, which were characterized by an abundant, dense network of microbial filaments forming bridges between grains (h, k). Patches of cement were also observed forming on these filament meshes (j). (l) Representative image of in situ beachrock, which was also characterized by dense bridges of filaments between adjacent ooids. Ooids in in situ beachrock were also intensely microbored.

Bacteriodetes, Firmicutes, Planctomycetes, and Chloroflexi at the phylum level (Figure 8a). The cyanobacterial taxa were dominated by ASVs from the orders Chroococcales and Pseudanabaenales (Figure 8b). Within the Chroococcales, the largest number of ASVs were from the Xenococcaceae, including a high number of ASVs from the genus *Chroococcidiopsis*, a UV- and desiccation-tolerant genus that is common in rock varnish communities (Daniela et al. 2000; Cockell et al. 2005; Fagliarone et al. 2017; Lacap-Bugler et al. 2017; Lingappa et al. 2021). Within the Pseudanabaenales, the largest number of ASVs were from the genus *Halomicronema*, a group characterized by 1-µm-thick filaments that form densely interwoven mats (Abed, Garcia-Pichel, and Hernández-Mariné 2002; Ruocco et al. 2018; Zupo et al. 2019; Lee et al. 2023). The general makeup of the microbial community from the in situ beachrock, both at the bacterial phylum level and at the cyanobacterial order level,

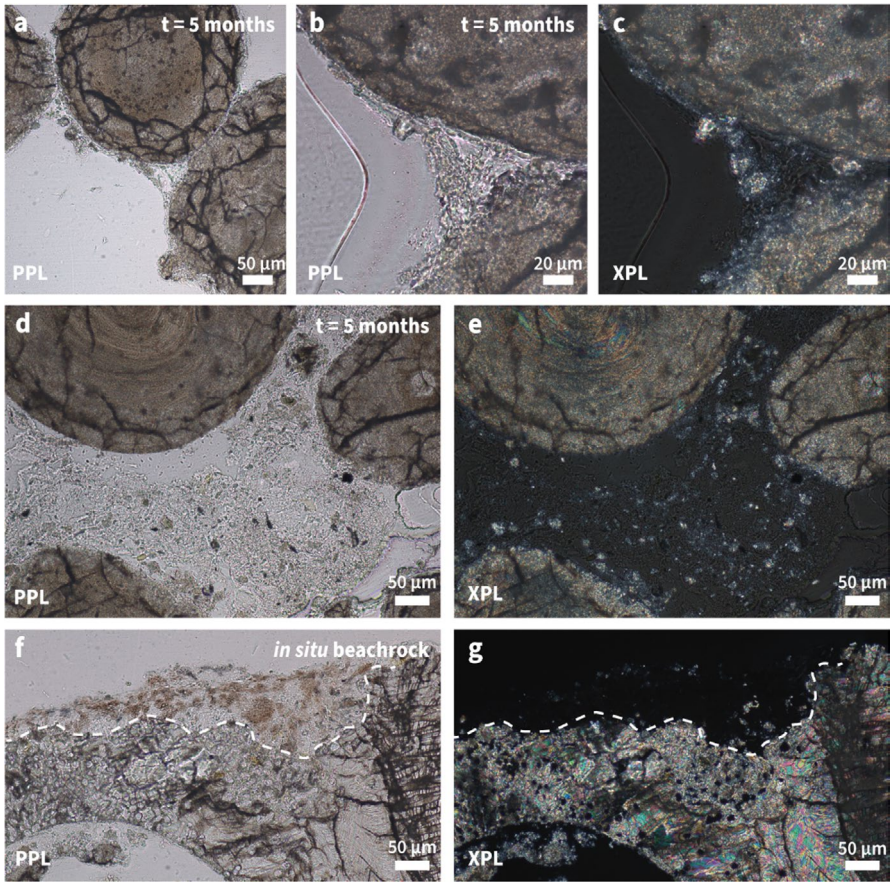


**FIGURE 6** | Plane- and cross-polarized transmitted light microscopy images of thin sections of 5-month incubation samples (a–e) and in situ beachrock sample (f, g). (a–c) Representative images of incipient meniscus cements formed along grain boundaries. Comparing plane-polarized light (PPL) and cross-polarized light (XPL) images (b, c) illustrates the presence of carbonate minerals (indicated by their birefringence in XPL image) in addition to microbial biomass at these grain boundaries. (d, e) Representative images of more continuous regions of microbial biomass and minerals (see birefringence in XPL image) between grains that were observed in some samples. (f, g) Example of in situ biofilm (area above white dashed line) sitting on the surface of an intensely microbored gastropod skeletal grain that was incorporated into the in situ beachrock. Endolith microboreholes are most visible as dark, uniformly extinct circular areas in the XPL image.

was all present in all field samples, even those incubated for only 4 days (Figure 8). The microbial communities in the field incubation samples clearly evolved over time, although the 5-month incubation samples were still distinct from the in situ beachrock (Figure 9).

## 4 | Discussion

### 4.1 | Rates of Beachrock Formation

Our observations demonstrate that the processes of biofilm colonization and cementation can both initiate rapidly, on timescales of days. Our 4-day field incubation samples revealed evidence of incipient meniscus cement formation (Figure 5a), suggesting that cementation could initiate after the wetting and drying from a few high tides. Similarly, at both the bacterial phylum level and within the phylum Cyanobacteria, the general makeup of the in situ beachrock microbial community was already present in the 4-day field incubation samples (Figure 8). At the same time, the 4-day field incubation samples were clearly not yet beachrock: the incipient meniscus cements in the 4-day field incubation samples were scarce and insufficient to hold grains together through the mild agitation of preparation of material for microscopy. Similarly, microscopy did not reveal any filaments analogous to those observed in 2.5-month and 5-month field incubation samples, demonstrating that there was comparably much less microbial biomass after only 4 days.

In contrast, our 5-month field incubation samples had many of the key characteristics of the in situ beachrock, including thick networks of interwoven cyanobacterial filaments forming bridges between adjacent grains and more extensive cement development (Figure 5i–k). The 5-month field incubation samples had higher TOC values than the control samples (Figure 7a), consistent with our qualitative observations that the nylon mesh became visually more green with increasing incubation time (Figure 4a,b). Although the most extensive biofilm colonization and incipient cementation were only a few grain diameters deep in each pouch, this is also analogous to the in situ beachrock. In the beachrock on Little Ambergris Cay, biofilm colonization (as reflected by dark green pigmentation) and cementation (as reflected by degree of induration) are also most intense in the uppermost few grain diameters below the surface (Figure 2b).

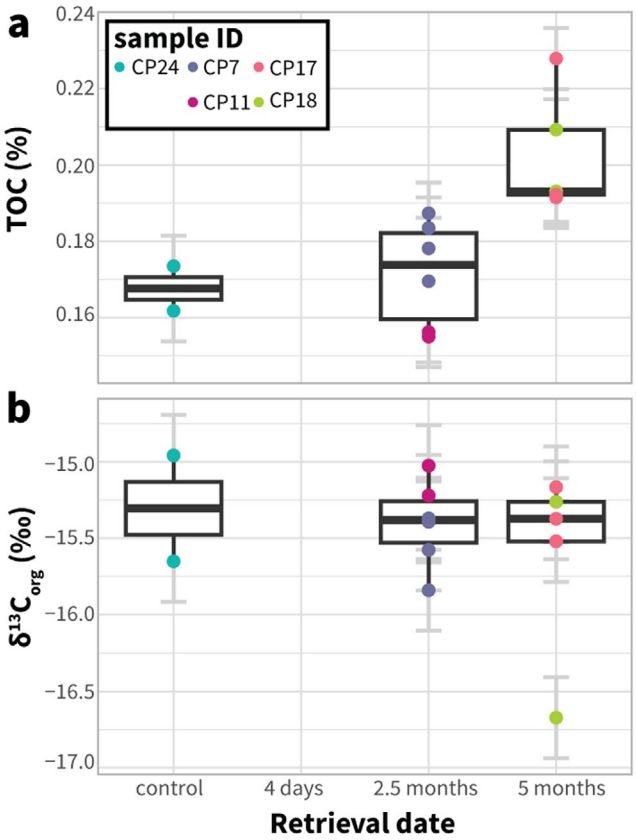


**FIGURE 7** | TOC (a) and $\delta^{13}C_{org}$ (b) values of ooids from control and field incubation samples. Each analysis is plotted by retrieval date on the *x* axis, including a control sample. Colors reflect sample identifier. We did not collect unrinsed samples for TOC analyses at the 4-day time point.

Overall, our results demonstrate that cementation and intense biofilm colonization in the upper intertidal zone can be extensive within a few months after fresh material is delivered (e.g., by a hurricane). Given that the Caicos platform experiences a tropical storm almost every year and a hurricane every several years (Wanless and Dravis 2008; McAdie et al. 2009), our field observations imply that detritus delivered by a large storm can be highly stabilized and indurated via incorporation into preexisting beachrock before the next large storm. This finding is also consistent with our observations of 20th-century anthropogenic detritus cemented into beachrock along the shorelines of Little Ambergris Cay (Figure 1g).

### 4.2 | Mechanisms of Beachrock Formation

Microbial metabolic processes are commonly implicated as promoting $CaCO_3$ precipitation by creating microenvironments that are more supersaturated with respect to $CaCO_3$ than ambient seawater or porewater (Dupraz et al. 2009; Diaz and Eberli 2022). Although beachrock formation has classically been considered a physicochemical process (Ginsburg 1953; Moore Jr 1973; Hanor 1978; Gischler and Lomando 1997), more recent studies have suggested that microbial activity might play a central role in beachrock formation through a few possible mechanisms that can increase $CaCO_3$ saturation state (McCutcheon et al. 2016, 2017; Diaz and Eberli 2022):

1. Boring microorganisms can pump $Ca^{2+}$ ions away from the mineral surface, increasing $[Ca^{2+}]$ in the adjacent solution.
2. EPS binds cations, including $Ca^{2+}$; consumption of EPS by heterotrophs later re-releases those cations, increasing $[Ca^{2+}]$ in the adjacent solution.
3. As a consequence of some types of microbial metabolic activity (e.g., by decreasing the total concentration of dissolved inorganic carbon—DIC—species via oxygenic photosynthesis).

The results of our experiments do not provide conclusive evidence that microbial metabolisms promoted $CaCO_3$ cementation. We cannot rule out the possibility that the biofilm community stimulated carbonate precipitation beyond what we would expect from abiotic processes alone; this would require a sterile end member of our experiment, and sterility is difficult to maintain over long periods of in situ field deployment. We observed meniscus cements after only 4 days, before there was any extensive biofilm development. These meniscus cements could be produced by abiotic processes. Caicos platform seawater is already supersaturated with respect to aragonite (Trower et al. 2018), and the degree of supersaturation would be further increased by evaporation and $CO_2$ degassing (Hanor 1978). Elevated daytime temperatures of surfaces in the upper intertidal zone would also promote rapid precipitation due to the temperature sensitivity of $CaCO_3$ precipitation kinetics (Romanek, Morse, and Grossman 2011). The dominantly aragonitic composition of incipient cements suggests that seawater is the dominant fluid involved in beachrock cementation. The detection of high-Mg calcite within incipient cements is also consistent with previous observations of mixed mineralogy (aragonite and high-Mg calcite) beachrock cements that formed in the marine phreatic zone (Moore Jr 1973; Gischler and Lomando 1997).

While we were not able to design an abiotic control experiment in the field, our experiments do demonstrate that biofilm development plays a significant role in beachrock formation on Little Ambergris Cay through the physical stabilization of sediment by microbial filaments. In the 2.5-month field incubation samples, grain size data (Table 1) show no evidence of a significant population of larger grains (i.e., individual ooids cemented together), but our SEM analyses revealed aggregates of ooids securely attached to the nylon mesh by the interwoven network of cyanobacterial filaments (Figure 5d). Similarly, a substantial portion of the material holding grains together in the 5-month field incubation samples is biomass rather than mineral (e.g., Figures 4i, 5d,e). Therefore, we propose that this sediment stabilization by biofilms leads to beachrock formation on Little Ambergris Cay because the network of microbial filaments can hold sediment in place as cementation proceeds. Although the nylon pouches kept the sand loosely contained, we interpret that the network of microbial filaments between grains played an important role in preventing grains from shifting around each other within the pouch, which would have broken delicate incipient cements. Although we did not observe clear evidence of microbially mediated carbonate mineral precipitation, it is possible that some of the incipient cements we observed in the 2.5-month and 5-month field incubation samples could have formed in association with EPS, as observed in previous studies (Neumeier 1999; McCutcheon et al. 2017).

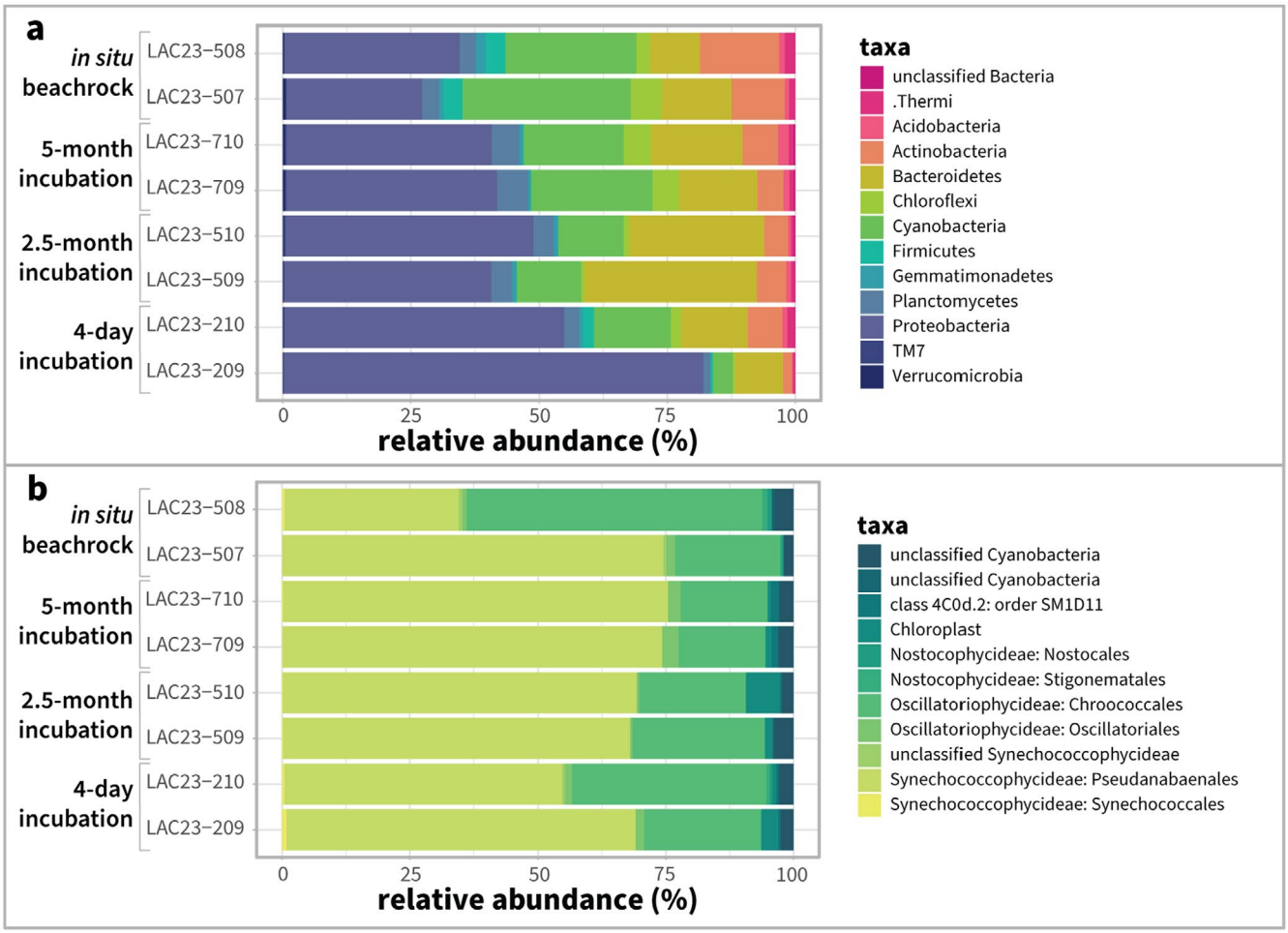


**FIGURE 8** | Bar charts comparing microbial communities observed in field incubation samples and in situ beachrock. (a) Bacterial phylum level comparison; only phyla with > 1000 ASVs are plotted for clarity. (b) Order level comparison within the phylum Cyanobacteria; only orders with > 100 ASVs are plotted for clarity.

Together, our microscopy and sequencing data suggest that *Halomicronema* is the primary genus responsible for this physical stabilization of sediment. *Halomicronema* is a genus of cyanobacteria with members that are known to have adaptations to low-light, high-salinity, and warm environments. *Halomicronema* is the dominant cyanobacterial genus in all but one sample (Figure 7b), and the morphological characteristics observed in our samples (e.g., Figure 6d–k) are comparable to previous descriptions in the literature as ~1-μm-thick unbranching filaments that form dense net-like mats (Abed, Garcia-Pichel, and Hernández-Mariné 2002; Ruocco et al. 2018; Zupo et al. 2019; Lee et al. 2023) and are capable of moving mm-scale distances within a microbial mat over a diel timescale (Fourçans et al. 2006). Furthermore, we note that *Halomicronema hongdechloris*, a cyanobacterium cultured from a stromatolite in Hamelin Pool (Shark Bay, Western Australia) (Chen et al. 2010), is known to produce chlorophyll *f* (Chl *f*), a red-shifted chlorophyll that would enable it to thrive in low-light conditions (Chen et al. 2010, 2012, 2019; Li et al. 2014; Schmitt et al. 2020). Although it is unknown if all members of the genus *Halomicronema* can produce Chl *f*, such an ability would be beneficial for a cyanobacterium living a cryptoendolithic lifestyle within a beachrock, where light is blocked by overlying sediment. Similarly, *Halomicronema excentricum* is known to be moderately halophilic (optimum growth at salinities of 32–120 ppt) and moderately thermophilic (optimum growth at temperatures between 28°C and 50°C) (Abed, Garcia-Pichel, and Hernández-Mariné 2002). Again, although we cannot confirm that the *Halomicronema* in our field site share these characteristics, these would also be advantageous traits for a cyanobacterium living in this environment, which is only submerged briefly every day and can reach much warmer temperatures than the adjacent subtidal environments.

The presence of *Chroococcidiopsis* in our samples is not surprising, given the well-documented UV- and desiccation tolerance of this genus (Daniela et al. 2000; Cockell et al. 2005; Fagliarone et al. 2017; Lacap-Bugler et al. 2017; Lingappa et al. 2021). However, we did not observe abundant cells morphologically consistent with this genus associated with aggregates of incipient beachrock. We suggest, therefore, that while *Chroococcidiopsis* can thrive in an extreme environment like a beachrock biofilm, our study provides no visual evidence that this genus plays a key role in beachrock development.

TOC analyses revealed that the ooid sediment already contained some organic carbon prior to field incubation

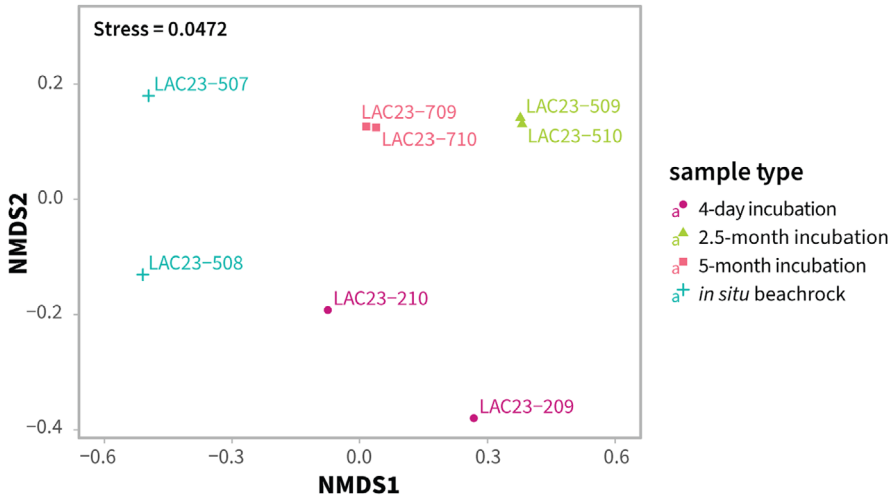


**FIGURE 9** | NMDS plot showing variance in microbial community as a function of incubation duration and compared with in situ beachrock samples.

experiments (Figure 7). It is likely that most of the organic carbon already in the ooid samples prior to field incubation was endolithic cyanobacterial biomass (Trower et al. 2018). The uniformity in $\delta^{13}C_{org}$ values over increasing field incubation time (Figure 7b) is consistent with the interpretation that cyanobacteria are the key primary producers in the beachrock biofilm, an inference consistent with our sequencing data (Figure 8).

### 4.3 | Implications for Coastal Resilience

Sandy coastlines are vulnerable to increased erosional events associated with anthropogenic climate change. The resilience of coastal systems is determined in part by the system's ability to retain sediment (Masselink and Lazarus 2019; Knight 2024). Mitigation efforts on sandy beaches include geoengineering of seawalls and beach nourishment, but these methods can lead to negative consequences for coastal ecosystems and commonly require repeated maintenance (Knight 2024). Management of these vulnerable coastlines should therefore also include nature-based solutions that increase stabilization of sediment while maintaining the community and integrity of the ecosystem (Knight 2024).

Previous studies have noted the potentially important role of beachrock formation as one of these potential nature-based solutions as it relates to coastal resilience. Due to its rapid cementation, beachrock formation 'locks' sediment into the beach profile, thus serving as a long-term sediment sink (Vousdoukas, Velegrakis, and Plomaritis 2007) and potentially preventing shoreline erosion through the stabilization of sediment (Kindler and Bain 1993; Chowdhury, Fazlul, and Hasan 1997; Dickinson 1999; Calvet et al. 2003; McCutcheon et al. 2016). Beyond its role in locking sediment into place, beachrock can also auto-repair through those same physicochemical and, in some cases, microbially mediated mechanisms (Danjo and Kawasaki 2013). If beachrock becomes submerged in the subtidal zone, it can still play a role in reducing the erosive energy of waves impacting the shoreline (Vousdoukas, Velegrakis, and Plomaritis 2007). Submerged beachrock may also expand the natural biodiversity in the rocky shore by providing more habitat for microorganisms, macroalgae, and fish (Saitis et al. 2022).

Rapid beachrock formation could be helpful to small reef islands, atolls, and low-lying carbonate systems like Little Ambergris Cay, which are especially vulnerable to the consequences of anthropogenic climate change, including sea level rise and increased intensity of storms (Knutson et al. 2010; Lin et al. 2012; Mendelsohn et al. 2012). Previous laboratory experiments have shown that microbial biofilms can play important roles in beachrock formation (Danjo and Kawasaki 2013; McCutcheon et al. 2017; Saitis et al. 2022); our study builds on this previous work by tracking these processes in the environment rather than in laboratory microcosms. The results of our in situ experiments demonstrate that biofilm colonization on fresh substrates occurs rapidly—within a few months—and can physically stabilize sediment, aiding in beachrock formation even when cementation is largely abiotic. These beachrock biofilms should therefore be considered useful and important agents in coastal resiliency. We recommend that future research examine larger-scale propagation of beachrock biofilm communities as a mechanism to help stabilize sandy shorelines.

#### Acknowledgments

We thank Paul Mahoney, James Seymour, and Shaun Austin for logistical support on Big Ambergris Cay; Emily Orzechowski and Andrew Knoll for providing field photos from previous field seasons; Ashley Maloney for assistance with organic carbon analyses; Usha Lingappa and Tori Cassady for advice on microscopy sample preparation; Jess Hankins for assistance with Raman microspectroscopy; and Sarah Preheim and Steven Wilbert for assistance with 16S rRNA gene sequencing. We are grateful to the Turks and Caicos Department of Environmental and Coastal Resources and the Turks and Caicos National Trust for allowing us to conduct research on Little Ambergris Cay under research permits SRP-2022-05-11-25 and SRP-2023-05-23-25. We acknowledge the analytical contributions of the CU Boulder Earth Systems Stable Isotope Lab (CUBES-SIL) Core Facility (RRID:SCR_019300). This research was supported by NSF grants OCE-2032129 (to EJT and MLG) and OCE-2307830 (to EJT,

MDC, and MLG). The sequencing data analysis was carried out at the Advanced Research Computing at Hopkins (ARCH) core facility (rockfish.jhu.edu), which is supported by the National Science Foundation (NSF) grant number OAC-1920103.

### Conflicts of Interest

The authors declare no conflicts of interest.

### Data Availability Statement

16S rRNA sequence data are available on the NCBI Sequence Read Archive database (https://www.ncbi.nlm.nih.gov/) under BioProject ID PRJNA1126140. The Python code used for sequencing data analysis is available at https://doi.org/10.5281/zenodo.11659019. The R code used for generating all plots is available at https://doi.org/10.5281/zenodo.12627716.

### References

Abed, R. M. M., F. Garcia-Pichel, and M. Hernández-Mariné. 2002. "Polyphasic Characterization of Benthic, Moderately Halophilic, Moderately Thermophilic Cyanobacteria With Very Thin Trichomes and the Proposal of *Halomicronema Excentricum* gen. nov., sp. nov." *Archives of Microbiology* 177: 361–370.

Bokulich, N. A., B. D. Kaehler, J. R. Rideout, et al. 2018. "Optimizing Taxonomic Classification of Marker-Gene Amplicon Sequences With QIIME 2's q2-Feature-Classifier Plugin." *Microbiome* 6: 90.

Bolyen, E., J. R. Rideout, M. R. Dillon, et al. 2019. "Reproducible, Interactive, Scalable and Extensible Microbiome Data Science Using QIIME 2." *Nature Biotechnology* 37: 852–857.

Callahan, B. J., P. J. McMurdie, M. J. Rosen, A. W. Han, A. J. A. Johnson, and S. P. Holmes. 2016. "DADA2: High-Resolution Sample Inference From Illumina Amplicon Data." *Nature Methods* 13: 581–583.

Calvet, F., M. C. Cabrera, J. C. Carracedo, et al. 2003. "Beachrocks From the Island of La Palma (Canary Islands, Spain)." *Marine Geology* 197: 75–93.

Cantine, M., E. Orzechowski, N. Stein, et al. 2024. "Rapid Growth of a Carbonate Island Over the Last Millennium." *Sedimentology* 71: 2119–2143.

Chen, M., M. A. Hernandez-Prieto, P. C. Loughlin, Y. Li, and R. D. Willows. 2019. "Genome and Proteome of the Chlorophyll f-Producing Cyanobacterium *Halomicronema Hongdechloris*: Adaptative Proteomic Shifts Under Different Light Conditions." *BMC Genomics* 20: 207.

Chen, M., Y. Li, D. Birch, and R. D. Willows. 2012. "A Cyanobacterium That Contains Chlorophyll f—a Red-Absorbing Photopigment." *FEBS Letters* 586: 3249–3254.

Chen, M., M. Schliep, R. D. Willows, Z.-L. Cai, B. A. Neilan, and H. Scheer. 2010. "A Red-Shifted Chlorophyll." *Science* 329: 1318–1319.

Chowdhury, S. Q., A. T. M. Fazlul, and H. K. Hasan. 1997. "Beachrock in St. Martin's Island, Bangladesh: Implications of Sea Level Changes on Beachrock Cementation." *Marine Geodesy* 20: 89–104.

Cockell, C. S., A. C. Schuerger, D. Billi, E. I. Friedmann, and C. Panitz. 2005. "Effects of a Simulated Martian UV Flux on the Cyanobacterium, *Chroococcidiopsis* sp. 029." *Astrobiology* 5: 127–140.

Cooper, J. A. G. 1991. "Beachrock Formation in Low Latitudes: Implications for Coastal Evolutionary Models." *Marine Geology* 98: 145–154.

Daniela, B., F. E. Imre, K. G. Hofer, C. M. Grilli, and O.-F. Roseli. 2000. "Ionizing-Radiation Resistance in the Desiccation-Tolerant Cyanobacterium *Chroococcidiopsis*." *Applied and Environmental Microbiology* 66: 1489–1492.

Danjo, T., and S. Kawasaki. 2013. "A Study of the Formation Mechanism of Beachrock in Okinawa, Japan: Toward Making Artificial Rock." *GEOMATE Journal* 5: 634–639.

Davies, P. J., and D. W. Kinsey. 1973. "Organic and Inorganic Factors in Recent Beach Rock Formation, Heron Island, Great Barrier Reef." *Journal of Sedimentary Research* 43: 59–81.

Diaz, M. R., and G. P. Eberli. 2022. "Microbial Contribution to Early Marine Cementation." *Sedimentology* 69: 798–822.

Dickinson, W. R. 1999. "Holocene Sea-Level Record on Funafuti and Potential Impact of Global Warming on Central Pacific Atolls." *Quaternary Research* 51: 124–132.

Dupraz, C., R. P. Reid, O. Braissant, A. W. Decho, R. S. Norman, and P. T. Visscher. 2009. "Processes of Carbonate Precipitation in Modern Microbial Mats." *Earth-Science Reviews* 96: 141–162.

Fagliarone, C., C. Mosca, I. Ubaldi, et al. 2017. "Avoidance of Protein Oxidation Correlates With the Desiccation and Radiation Resistance of Hot and Cold Desert Strains of the Cyanobacterium *Chroococcidiopsis*." *Extremophiles: Life Under Extreme Conditions* 21: 981–991.

Falkenroth, M., A. N. Green, J. A. G. Cooper, M. D. Menzel, and G. Hoffmann. 2022. "Breaking Up and Making Up – Reworking of Holocene Calcarenite Platform Into Rapidly-Forming Beachrock Breccias on a High Energy Coastline (St. Lucia, South Africa)." *Sedimentology* 69: 1339–1364.

Flügel, E. 2010. *Microfacies of Carbonate Rocks: Analysis, Interpretation and Application*. Berlin, Heidelberg, Germany: Springer.

Fourçans, A., A. Solé, E. Diestra, et al. 2006. "Vertical Migration of Phototrophic Bacterial Populations in a Hypersaline Microbial Mat From Salins-de-Giraud (Camargue, France)." *FEMS Microbiology Ecology* 57: 367–377.

Ginsburg, R. N. 1953. "Beachrock in South Florida." *Journal of Sedimentary Research* 23: 85–92.

Gischler, E., and A. J. Lomando. 1997. "Holocene Cemented Beach Deposits in Belize." *Sedimentary Geology* 110: 277–297.

Hanor, J. S. 1978. "Precipitation of Beachrock Cements; Mixing of Marine and Meteoric Waters vs. $CO_2$-Degassing." *Journal of Sedimentary Research* 48: 489–501.

Katoh, K., K. Misawa, K.-I. Kuma, and T. Miyata. 2002. "MAFFT: A Novel Method for Rapid Multiple Sequence Alignment Based on Fast Fourier Transform." *Nucleic Acids Research* 30: 3059–3066.

Kindler, P., and R. J. Bain. 1993. "Submerged Upper Holocene Beachrock on San Salvador Island, Bahamas: Implications for Recent Sea-Level History." *Geologische Rundschau: Zeitschrift Fur Allgemeine Geologie* 82: 241–247.

Knight, J. 2024. "Nature-Based Solutions for Coastal Resilience in South Africa." *South African Geographical Journal, Being a Record of the Proceedings of the South African Geographical Society* 106: 21–50.

Knutson, T. R., J. L. McBride, J. Chan, et al. 2010. "Tropical Cyclones and Climate Change." *Nature Geoscience* 3: 157–163.

Lacap-Bugler, D. C., K. K. Lee, S. Archer, et al. 2017. "Global Diversity of Desert Hypolithic Cyanobacteria." *Frontiers in Microbiology* 8: 867.

Lee, H. E., J. H. Lee, S. M. Park, and D. G. Kim. 2023. "Symbiotic Relationship Between Filamentous Algae (*Halomicronema* sp.) and Extracellular Polymeric Substance-Producing Algae (*Chlamydomonas* sp.) Through Biomimetic Simulation of Natural Algal Mats." *Frontiers in Microbiology* 14: 1176069.

Li, Y., Y. Lin, P. C. Loughlin, and M. Chen. 2014. "Optimization and Effects of Different Culture Conditions on Growth of *Halomicronema Hongdechloris*—a Filamentous Cyanobacterium Containing Chlorophyll f." *Frontiers in Plant Science* 5: 67.

Lin, N., K. Emanuel, M. Oppenheimer, and E. Vanmarcke. 2012. "Physically Based Assessment of Hurricane Surge Threat Under Climate Change." *Nature Climate Change* 2: 462–467.

Lingappa, U. F., C. M. Yeager, A. Sharma, et al. 2021. "An Ecophysiological Explanation for Manganese Enrichment in Rock Varnish." *Proceedings of the National Academy of Sciences of the United States of America* 18: 118.

Masselink, G., and E. Lazarus. 2019. "Defining Coastal Resilience." *Watermark* 11: 2587.

Mauz, B., M. Vacchi, A. Green, G. Hoffmann, and A. Cooper. 2015. "Beachrock: A Tool for Reconstructing Relative Sea Level in the Far-Field." *Marine Geology* 362: 1–16.

McAdie, C. J., C. W. Landsea, C. J. Neumann, J. E. David, E. S. Blake, and G. R. Hammer. 2009. *Tropical Cyclones of the North Atlantic Ocean, 1851–2006* (No. Historical Climatology Series 6-2). Asheville, NC, USA: National Climatic Data Center.

McCutcheon, J., L. D. Nothdurft, G. E. Webb, D. Paterson, and G. Southam. 2016. "Beachrock Formation via Microbial Dissolution and Re-Precipitation of Carbonate Minerals." *Marine Geology* 382: 122–135.

McCutcheon, J., L. D. Nothdurft, G. E. Webb, et al. 2017. "Building Biogenic Beachrock: Visualizing Microbially-Mediated Carbonate Cement Precipitation Using XFM and a Strontium Tracer." *Chemical Geology* 465: 21–34.

McDonald, D., M. N. Price, J. Goodrich, et al. 2012. "An Improved Greengenes Taxonomy With Explicit Ranks for Ecological and Evolutionary Analyses of Bacteria and Archaea." *ISME Journal* 6: 610–618.

Mendelsohn, R., K. Emanuel, S. Chonabayashi, and L. Bakkensen. 2012. "The Impact of Climate Change on Global Tropical Cyclone Damage." *Nature Climate Change* 2: 205–209.

Moore, C. H., Jr. 1973. "Intertidal Carbonate Cementation Grand Cayman, West Indies." *Journal of Sedimentary Research* 43: 1210.

Neumeier, U. 1999. "Experimental Modelling of Beachrock Cementation Under Microbial Influence." *Sedimentary Geology* 126: 35–46.

Orzechowski, E. A., J. V. Strauss, and A. H. Knoll. 2016. "Age and Construction of Little Ambergris Cay Bedrock Rim, Southeastern Caicos Platform, British West Indies." AGU Fall Meeting.

Preheim, S. P., A. R. Perrotta, A. M. Martin-Platero, A. Gupta, and E. J. Alm. 2013. "Distribution-Based Clustering: Using Ecology To Refine the Operational Taxonomic Unit." *Applied and Environmental Microbiology* 79: 6593–6603. https://doi.org/10.1128/aem.00342-13.

Price, M. N., P. S. Dehal, and A. P. Arkin. 2010. "FastTree 2—Approximately Maximum-Likelihood Trees for Large Alignments." *PLoS One* 5: e9490.

Romanek, C. S., J. W. Morse, and E. L. Grossman. 2011. "Aragonite Kinetics in Dilute Solutions." *Aquatic Geochemistry* 17: 339–356.

Ruocco, N., M. Mutalipassi, A. Pollio, S. Costantini, M. Costantini, and V. Zupo. 2018. "First Evidence of *Halomicronema Metazoicum* (Cyanobacteria) Free-Living on *Posidonia oceanica* Leaves." *PLoS One* 13: e0204954.

Saitis, G., A. Karkani, E. Koutsopoulou, K. Tsanakas, S. Kawasaki, and N. Evelpidou. 2022. "Beachrock Formation Mechanism Using Multiproxy Experimental Data From Natural and Artificial Beachrocks: Insights for a Potential Soft Engineering Method." *Journal of Marine Science and Engineering* 10: 87.

Schmitt, F.-J., Z. Y. Campbell, M. Moldenhauer, and T. Friedrich. 2020. "Light-Induced Phycobilisome Dynamics in *Halomicronema Hongdechloris*." *Journal of Photochemistry and Photobiology. A, Chemistry* 403: 112838.

Shinn, E. A. 1969. "Submarine Lithification of Holocene Carbonate Sediments in the Persian Gulf." *Sedimentology* 12: 109–144.

Stein, N. T., J. P. Grotzinger, D. P. Quinn, et al. 2023. "Geomorphic and Environmental Controls on Microbial Mat Fabrics on Little Ambergris Cay, Turks and Caicos Islands." *Sedimentology* 70: 1915–1944.

Trower, E. J., M. D. Cantine, M. L. Gomes, et al. 2018. "Active Ooid Growth Driven by Sediment Transport in a High-Energy Shoal, Little Ambergris Cay, Turks and Caicos Islands." *Journal of Sedimentary Research* 88: 1132–1151.

Vousdoukas, M. I., A. F. Velegrakis, and T. A. Plomaritis. 2007. "Beachrock Occurrence, Characteristics, Formation Mechanisms and Impacts." *Earth-Science Reviews* 85: 23–46.

Wanless, H. R., and J. J. Dravis. 2008. "Role of Storms and Prevailing Energy in Defining Sediment Body Geometry, Composition, and Texture on Caicos Platform." In *Developing Models and Analogs for Isolated Carbonate Platforms-Holocene and Pleistocene Carbonates of Caicos Platform, British West Indies*, 13–20. Tulsa, OK: SEPM.

Zupo, V., M. Mutalipassi, N. Ruocco, et al. 2019. "Distribution of Toxigenic *Halomicronema* spp. in Adjacent Environments on the Island of Ischia: Comparison of Strains From Thermal Waters and Free Living in *Posidonia Oceanica* Meadows." *Toxins* 11: 549.

## Supporting Information

Additional supporting information can be found online in the Supporting Information section.